Int. J. Electrochem. Sci., 15 **(2020)** 4188 – 4202, doi: 10.20964/2020.05.22

International Journal of
ELECTROCHEMICAL
SCIENCE
www.electrochemsci.org

Electrochemical Study of a Three-dimensional Zn-Mn Alloy//Mn-doped Polyaniline Suspension Flow Battery with Enhanced Electrochemical Performance

Huijun Cao[1,2], *Shihui Si*[1,*], *Xiangbin Xu*[2], *Xiaoyu Yang*[2], *Jiufeng Liu*[2], *Sen Wu*[1]

[1] College of Chemistry and Chemical Engineering, Central South University, Changsha 410083, PR China
[2] Department of Pharmaceutical and bioengineering, Hunan Chemical Vocational Technology College, Zhuzhou 412004, PR China
[*]E-mail: sishihui@163.com

Received: 16 September 2019 / *Accepted:* 11 February 2020 / *Published:* 10 April 2020

The electrochemical activities of polyaniline (PANI) in different manganese (Mn) salt solutions were studied. The experimental results show better electrochemical activity for PANI in the manganese chloride ($MnCl_2$) solution. Additionally, the electrochemical reaction performance of PANI was enhanced by the addition of lithium chloride (LiCl) in the $MnCl_2$ electrolyte. Doping with manganese ions (Mn^{2+}) also improved the conductivity of $MnCl_2$. Porous carbon felt was used as the three-dimensional (3D) matrix for electrochemical sedimentation. The deposition efficiency was greatly improved by the addition of zinc ions (Zn^{2+}) in the electrolyte. With a concentration of 0.5 M Zn^{2+}, the deposition efficiency of Mn was 93%. With the Mn-doped PANI particle suspension as the cathode material and the 3D Zn-Mn alloy as the anode, the flow battery was tested at different charge and discharge current densities. The discharge capacity density reached 153 $mAh\cdot g^{-1}$ at 15 mA cm^{-2}, and the average discharge voltage was more than 1.2 V, which indicates that the present cell is promising for use as high-performance rechargeable battery or energy storage.

Keywords: Electrolyte with Li^+ additive, 3D Zn-Mn alloy anode supported by porous carbon felt**,** Coelectrodeposition**,** Mn-doped PANI particle suspension, Low corrosion

1. INTRODUCTION

As an electrode material for energy storage, the macromolecule PANI has attracted considerable attention due to its excellent environmental stability, controllable electrical conductivity, interesting redox properties and nontoxicity[1-6]. A rechargeable battery was designed using a PANI conductive suspension as the cathode active material and metal Zn as the anode[7-11]. The properties of the PANI suspension can be further enhanced by modification or doping to improve the battery performance[12-

15]. PANI in an acidic aqueous system possesses strong stability, but the Zn anode suffers from corrosion and surface dendrite formation[16-17]. Although Zn offers distinct advantages as an anode material, the Zn//PANI rechargeable battery has a low operating voltage and an average discharge voltage of only approximately 0.7 V. An anode material that can function in an aqueous system, Mn, has properties similar to those of Zn. In addition, the standard potential of Mn is 0.42 V higher than that of Zn. Thus, an electrode pair of Mn and PANI offers a higher operating voltage than a Zn system[18-26].

In this study, the electrochemical performance of PANI in different manganese salt solutions was investigated. To examine the influence of Li^+ and Mn^{2+} on PANI activity, LiCl was introduced into the electrolyte, and $MnCl_2$ was used in the electrosynthesis of PANI. Li^+ doping and Mn^{2+} doping increased the electrochemical activity of PANI. The 3D carbon-supported Zn-Mn anode was prepared by Zn and Mn coelectrodeposition on a porous carbon felt substrate. The 3D Zn-Mn anode was combined with a PANI conductive suspension into a flow battery. The current efficiency of the Zn-Mn coelectrodeposition on the carbon felt was evaluated by chronocoulometry. An energy storage system was designed that used a Mn-doped PANI conductive suspension as the active cathode material for a 3D Zn-Mn alloy rechargeable battery.

2. EXPERIMENTAL SECTION

2.1 Preparation of PANI suspension

Referring to these papers[11-14, 27-30], the graphite plate electrode was mechanically polished with 0.5 μm alumina with polishing cloths and then cleaned in an ultrasonic bath in a water/ethanol mixture. PANI powder was synthesized galvanostatically on a pretreated graphite plate (5.0 cm × 5.0 cm) in a solution containing 1.0 M $HClO_4$ and 0.25 M aniline at a current density of 5.0 $mA\cdot cm^{-2}$. After the synthesis, the PANI powder was removed by scratching with a plastic knife. Ultimately, the PANI powder was washed with diluted water. To obtain microsized PANI powder, the obtained powder was subjected to grinding using a cutting mill for 20 min and then dried at 80 °C for 24 h in a vacuum oven.

The PANI suspensions were prepared by dispersing the prepared PANI microparticles into a manganese salt solution. To investigate the electrochemical performance of PANI in different systems, $MnSO_4$, $MnCl_2$, or $Mn(CH_3COO)_2$ solutions were used. The influence of LiCl on PANI in solution was also studied.

2.2 Preparation of PANI film

The flexible graphite paper was soaked in concentrated nitric acid for 24 h, cleaned with distilled water and then weighed after being air dried. The PANI films were electrochemically grown on pretreated flexible graphite paper substrates (1.0 cm×1.0 cm) in 0.25 M aniline and 1.0 M $HClO_4$ solution and at a 5.0 $mA\cdot cm^{-2}$ current density for 30 min. The obtained PANI film electrodes were washed with 1.0 M $HClO_4$ followed by deionized water and then air dried and weighed, referring to these papers[31-33].

Cyclic voltammetry (ν=50 $mV\cdot s^{-1}$) measurements were performed between -0.20 V and 0.80 V, and the PANI film was grown on the pretreated Au electrode, which was mechanically polished with 0.5 μm alumina with polishing cloths and then cleaned in an ultrasonic bath in a water/ethanol mixture[34,35]. After polymerization, the PANI film deposited on the surface of the Au electrode was rinsed with 1.0 M $HClO_4$ followed by deionized water.

2.3 Preparation of 3D Zn-Mn alloy electrode

By linear sweep voltammetry, the electrodeposition behavior (between -0.6 V and -1.8 V) of Zn^{2+}, Mn^{2+} and Zn^{2+}+Mn^{2+} in an aqueous chloride salt-citrate system was investigated with porous carbon felt as the operating electrode, platinum wire as the counter electrode covered with anion membrane and a saturated calomel electrode (SCE) as the reference electrode, a salt bridge with a Luggin capillary used to eliminate the liguid junction potential between different solution. The 3D Zn-Mn alloy electrode was prepared by coelectrodeposition on a carbon felt substrate in $MnCl_2$ solution with added $ZnCl_2$ [36-38]. A copper coulomb meter was used to record the total amount of electricity in the cathode reaction. Atomic absorption and spectrophotometric methods were used to analyze the Zn and Mn content in deposits and electrolyte solution, respectively. The influence of the Zn^{2+} atomic concentration (at%) /Mn^{2+} at% and total at% of Zn^{2+}+Mn^{2+} in solution on the deposition current efficiency and Mn at% in the deposition layer was investigated. Ultimately, the current efficiency for deposition was calculated by subtracting the current density related to H_2 evolution from the total current density employed. After condition optimization, the 3D Zn-Mn alloy electrode supported by porous carbon felt was obtained potentiostatically with electrolyte solution containing 0.3M $MnCl_2$, 0.1 M $ZnCl_2$, 0.6 M sodium citrate (Na_3Ct), 0.4 M boric acid (H_3BO_3), 0.2 M potassium chloride (KCl), amount of aloe vera as bio-plasticizer at 30℃ temperature, pH 6, and the cathode current density (j_c) of 3.5 $A.dm^{-2}$.

2.4 3D Zn-Mn alloy//Mn-doped PANI suspension flow battery

To investigate the electrochemical performance of a 3D Zn-Mn alloy//PANI suspension flow battery, a reasonable flow cell system was designed (as shown in Fig. 1). The flow battery consisted of an energy storage unit and an energy conversion unit. A storage tank and single pump composed the energy storage unit, and the energy conversion unit was the cell. A smooth graphite plate recessed in a notch (4.0 cm×1.0 cm×0.5 cm) of a polytetrafluoroethylene (PTFE) plate was used as the positive current collector.

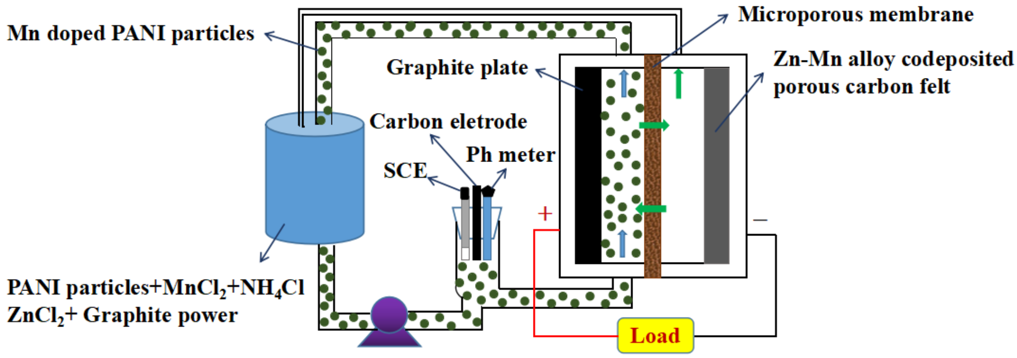

Figure 1. Schematic illustration of the battery system.

The flowing Mn-doped PANI suspension (containing 20% graphite powder vs PANI) played the role of the cathode and catholyte (pH 3.5). A 3D Zn-Mn alloy plate (4.0 cm^2 area) was used as the anode. Between the cathode and anode compartments, a polypropylene microporous membrane with a mean pore size of 0.45 μm, thickness of 0.18 mm, and active area of 4.0 cm×1.0 cm served as the separator to prevent PANI particles from entering the anode compartment. The electrolyte in the battery was an aqueous solution containing 0.3 M $MnCl_2$, 0.5 M $ZnCl_2$, 0.3 M NH_4Cl, and 0.1 M LiCl. During battery operation, the Mn-doped PANI suspension was pumped into the cathode compartment at 37.5 mL min^{-1}, and part of the electrolyte penetrated the anode compartment via the microporous membrane. The remaining electrolyte and PANI particles that passed through the cathode compartment returned to the storage tank. The active material of the two electrodes could be regenerated simultaneously in a single flow battery design.

2.5. Electrochemical characterization

All electrochemical experiments were carried out with a CHI660D electrochemical analyzer (Chenhua Instrument Co., China). The working electrode was PANI film with Au (with a diameter of 2.0 mm) as the current collector or a graphite plate, platinum wire as the counter electrode, and SCE as the reference electrode. All potentials were referenced to the SCE. All charge/discharge experiments on the 3D Zn-Mn alloy//Mn-doped PANI suspension flow battery were conducted with a BTS battery test system (Neware Ltd., China). All solution pH measurements were performed using a digital pH meter (PHS-3G, Shanghai Leici Instrument Factory, China). A JEOLJSM-6360F scanning electron microscopy service was used to obtain scanning electron microscopy images of the Zn-Mn deposition layer.

3. RESULTS AND DISCUSSION

3.1 Influence of anions on the electrochemical performance of PANI

Fig. 2 shows the comparative cyclic voltammograms of the PANI film at the Au electrode in 0.3 M $MnSO_4$, 0.3 M $MnCl_2$, and 0.3 M $Mn(CH_3COO)_2$. Compared to $MnSO_4$ and $MnCl_2$ aqueous solutions, PANI has low electrochemical activity in the Mn($CH_3COO)_2$ system and displays minimal redox peaks. However, in the $MnSO_4$ solution system, PANI exhibits a powerful electrochemical reply with a high peak current but with a poor peak shape, and the redox peak potentials diverge from those of PANI, and two pairs of peaks overlap. In contrast, in $MnCl_2$ medium, there are two obvious redox peaks with high peak current, which illustrates that the redox electrochemical property of PANI in that system is the best of all. This result may explain the conspicuous divergence of the radius size of anions [39-40]. The PANI redox reaction is a process of doping and dedoping. The doping rate directly depends on the anion radius. Among the three anions, acetate ions have the largest radius, leading to great steric hindrance in the doping process. Sulfate ions are next, and then, chloride ions possess the smallest radius, which results in the least steric hindrance. Consequently, doping and dedoping occur smoothly for the chloride ions, so the highest electrochemical activity of PANI was observed in the $MnCl_2$ solution.

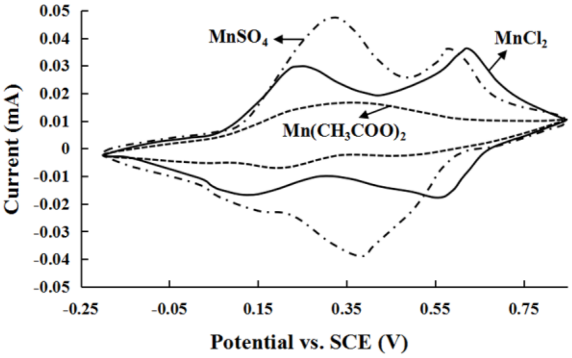

Figure 2. Cyclic voltammograms of PANI film grown on a gold electrode with a diameter of 2 mm in different electrolytes at a scan rate of 50 mV s^{-1}.

3.2 Influence of lithium ions on the electrochemical performance of PANI

The electrochemical activity of PANI relates to the acidity of the medium [18, 41]. The higher the solution acidity, the higher the activity of PANI. Therefore, one expectation might be that higher electrolyte acidity would increase the activity. However, the acidity of the electrolyte solution cannot increase beyond a certain threshold because high acidity easily leads to metal corrosion with self-discharging, resulting in a large negative impact on metal cation deposition on the negative electrode. For example, the optimal pH value for Mn electrodeposition was within the range of 6.8-7.3, but PANI has poor electrochemical activity in this range, even acting as an insulator.

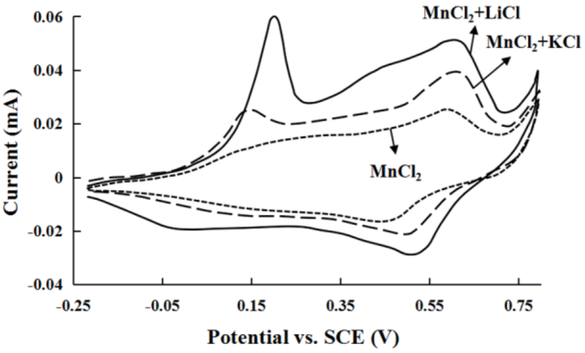

Figure 3. Cyclic voltammograms of PANI film with added $MnCl_2$ and different additives, gold electrode with diameter of 2 mm, scan rate 50 mV s^{-1}.

Thus, the electrolyte was improved by the addition of LiCl, taking advantage of the similarity in size and the embedding and de-embedding properties of Li^+ and H^+[42-44]. Fig. 3 shows the cyclic voltammograms of PANI in $MnCl_2$ solution with or without additives. As shown in Fig. 3, K^+ or Li^+ significantly enhanced the electroactivity of PANI. In particular, Li^+ doubled the currents of the first pair of redox peaks compared to the original currents in the absence of Li^+. Although the electroactivity of PANI was strengthened by the addition of K^+ and Li^+, the mechanisms are obviously different. The increase with K^+ is due to the increase in the ion concentration in the solution, which increases the conductivity of the solution. The addition of Li^+ ions improved the solution conductivity, and the ions also participated in the doping and dedoping of PANI. Thus, in the case of a low acidity solution, the electroactivity of a $MnCl_2$ electrolyte solution can be improved by the addition of Li^+ ions. For the PANI suspension flow battery, the use of a LiCl additive can also inhibit aggregation of the PANI particles.

3.3 The electrochemical behavior of Mn-doped PANI

During preparation of the PANI film by electropolymerization, $MnCl_2$ was added to produce Mn-doped PANI. Fig. 4 shows the cyclic voltammograms of Mn-doped PANI with various concentrations of $MnCl_2$ solution. As shown in Fig. 4, for a Mn^{2+} concentration of 0.1 M, the Mn doping had only a minor influence on the electroactivity of PANI. With the increasing Mn^{2+} concentration, the peak current increased rapidly. Beyond a doping concentration of 0.3 M, the Mn^{2+} concentration increased, but the peak current showed little change, which indicates the Mn^{2+} doping in PANI reaches saturation at this concentration[45, 46]. Thus, further addition of $MnCl_2$ cannot further improve PANI activity. Mn doping affects the PANI electrochemical performance due to the combination of the empty orbital of the transition metal and the imino group of PANI[47-49]. Nitrogen atoms in PANI with anthraquinone-type structures supply electrons to the transition metal, forming π bonds. The doping metal ions are not only adsorbed on the surface of the PANI particles but also enter the PANI molecular chains. Metal doping is a pseudoprotonated process in which the formation of a strong π bond allows electrons to transfer easily along the PANI molecular chain, increasing the conductivity and elevating the external electroactivity of PANI[40]. Electrochemical impedance spectroscopy was used to test the Mn^{2+}-doped PANI samples with various concentrations of Mn^{2+}, as shown in Fig. 5. The Nyquist plots reveal a 45° angle between the undoped PANI curve and the χ axis at low frequency, which illustrates that in solution the ion diffusion controls the resistance. The χ axis intercept in the high-frequency region is the equivalent series resistance (ESR)[50]. As the doping Mn^{2+} concentration increased, the ESR in the high-frequency region significantly decreased, and the slope of the line in the low-frequency region increased, which suggests capacitance behavior. The results demonstrate the conductivity of the Mn-doped PANI material greatly increases as the concentration of doped Mn^{2+} increases.

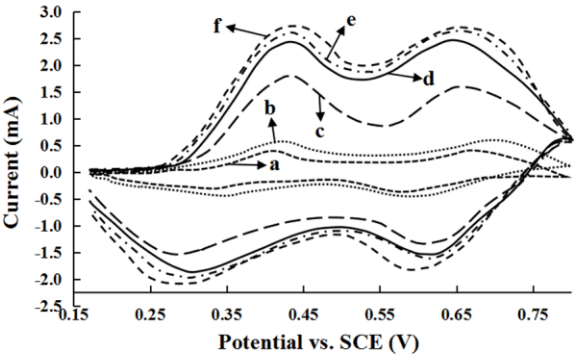

Figure 4. Cyclic voltammograms of Mn-doped PANI with various concentrations of $MnCl_2$ solution. (a), pure PANI (b), PANI + 0.1 M $MnCl_2$ (c), PANI + 0.2 M $MnCl_2$ (d), PANI + 0.3 M $MnCl_2$ (e), PANI + 0.4 M $MnCl_2$ (f), PANI + 0.5 M $MnCl_2$.

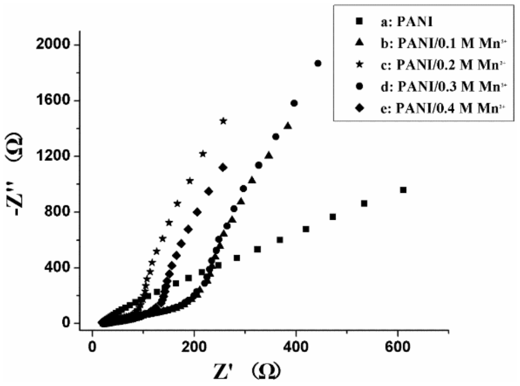

Figure 5. AC impedance spectroscopy for various concentrations of Mn-doped PANI.

3.4 Zn-Mn coelectrodeposition behavior

Because of the high dissolution rate of a pure Zn coating, various Zn-based alloys are commonly used to protect mild steel from corrosion[51-52]. Among the various Zn-based binary and ternary alloys, the electrodeposits of Zn-Ni[53-54], Zn-Ni-Cd[55-57], Zn-Fe[58-59] and Zn-Co[60-61] has received the most attention in industry. Recently, Zn-Mn has been found to have markedly attractive corrosion performance[62-63,36-38]. According to the literature, research has focused on Zn-Mn alloy electrodeposits as a high-performance sacrificial electroplated coating and the influence of the Mn^{2+} concentration on Zn-Mn electrodeposis. However, no data have been reported on the molar ratio of Zn^{2+}/Mn^{2+}, total $Zn^{2+}+Mn^{2+}$ concentration and additives influence on Zn-Mn coelectrodeposits and deposition utilization as anodes of rechargeable batteries. In this work, an attempt was made to gain insight into the electrochemical performance, morphology and structure of Zn-Mn coelectrodeposits from a chloride electrolyte with porous carbon felt as the operating electrode. 0.2M KCl solution was used as basic electrolyte, Aloe vera as bio-plasticizer, boric acid as a buffer which could bring the Zn^{2+} and Mn^{2+} deposition potentials closer and could move the overpotential for H_2 evolution positively and could restrain the evolution of H_2, leading to improved current efficiency of Zn-Mn coelectrodeposition. Na_3Ct was employed as complex agent, which provided the ability of pulling down the electrodeposition potential of Zn and Mn. The anode was covered anion membrane, which prevented the oxide reaction of Mn^{2+} on anode and favored the enlarging of cathode current efficiency.

From the partial current curves of Zn (i_{Zn}) and H_2 (i_{H_2}) in Fig.6(A), Zn^{2+} begins to electrodeposit on porous carbon felt at -1.36 V. The Zn^{2+} eletrodeposition prevents the partial current of H^+ from increasing. After exceeding -1.50 V, the partial current of Zn decreases. When the cathodic potential exceeds -1.57 V, the i_{H_2} increases sharply, and a large amount of H_2 is precipitated. Fig.6(B) shows the difference between the partial current value of Mn (i_{Mn}) and H_2 (i'_{H_2}) is not large. The eletrodeposition potential of Mn is about -1.4V, which is approximately consistent with previous studies[40, 64-65]. After -1.65V, the i'_{H_2} exceeds the i_{Mn}, which indicates that a large amount of H_2 evolution is accompanied by the electrodeposition of Mn on cathode. Also because the overpotential of hydrogen on metallic Mn is significantly smaller than the overpotential of metallic Zn, which is the reason for the low current efficiency of Mn deposition. The polarization curve of Zn-Mn alloy lies between the polarization curves of Mn and Zn, which is actually the sum of the reduction currents of the Zn^{2+}, Mn^{2+}, and H^+ on cathodes, as showed in Fig.6C. It is preliminarily determined that the reason for the low current efficiency of Zn^{2+}+Mn^{2+} coelectrodeposition is hydrogen evolution on cathode.

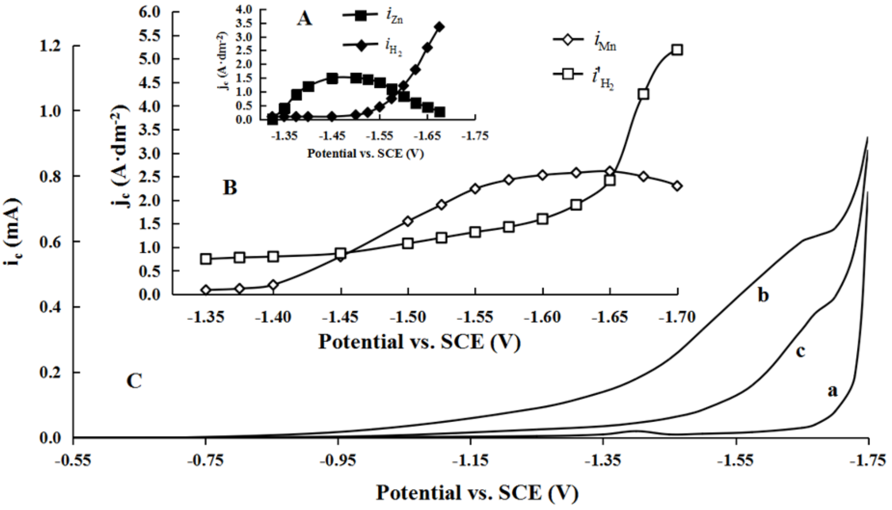

Figure 6. Steady-state polarization curves and the partial current polarization curves obtained at 30℃ temperature and pH 6 with Linear potential scanning method from negative to positive in the solution containing 0.6 M Na_3Ct, 0.4 M H_3BO_3, 0.2 M KCl and A: 0.1 M $ZnCl_2$; B, 0.3 M $MnCl_2$; C, a, 0.1 M $ZnCl_2$; b, 0.3 M $MnCl_2$; c, 0.1 M $ZnCl_2$+0.3 M $MnCl_2$

It is found by salt spray test that the corrosion resistance of the corrosion resistance of Zn-Mn alloy increases with the increase of the Mn content in the deposition layer[66]. The Mn at% is less than 20%, and its corrosion resistance is not much different from that of the pure Zn deposition layer. When the Mn at% is less than 35%, there are many micropores in the layer and the corrosion resistance is low. The Mn at% is higher than 40%, and the corrosion resistance is no longer significantly improved. Therefore, the Mn at% is preferably 30% to 45%.

Fig.7a shows the relationship between the total Zn^{2+}+Mn^{2+} concentration and the Mn at% in deposition layer at the molar ratio 1/3 constantly of Zn^{2+} to Mn^{2+} in the electrolyte solution. The Mn at% in layer decreases with the increase of the total Zn^{2+}+Mn^{2+} concentration, which is mainly due to the increase in the absolute concentration of Zn^{2+} simultaneously. It indicates that Zn^{2+} are easier to obtain electrons than Mn^{2+}, and the cathode reduction reaction rate of Zn^{2+} is greater than Mn^{2+}, so the Zn at% increase is greater than that of Mn in layer. Concequently, the Zn at% and Mn at% in the layer are not increased in proportion, and the increment of Zn at% increase is greater than that of Mn, the Mn at% in the layer decreases with the increase of the total concentration of Zn^{2+}+Mn^{2+} in the solution. Therefore, in order to obtain a suitable Mn at% in layer, the total concentration of Zn^{2+}+Mn^{2+} and the molar ratio of Zn^{2+} to Mn^{2+} in the solution must be kept within a suitable range, That is: in the case of increasing the total concentration of Zn^{2+}+Mn^{2+}, to keep the Mn at% in layer unchanged, the molar ratio of Mn must be increased. Although the Mn at% in the layer could be increased by increasing the cathode current density (j_c), the appearance of deposits is deteriorated which is contributed by amount of H_2 evolution. So the appropriate range of total Zn^{2+}+Mn^{2+} concentration is 0.35 M to 0.5 M.

Fig.7e shows the effect of different molar ratios of Mn^{2+} to Zn^{2+} in the electrolyte solution on the Mn at% in the deposition layer. When the molar ratio was less than 1/5, the Mn at% in the deposition layer stays lowly. Then the Mn at% slowly rised between 3/7 and 1/1. When the molar ratio reaches more than 3/2, the Mn at% in the deposition layer rises rapidly which results in H_2 generating. So the appropriate molar ratio resides selectively about 11/9, which render the Mn at% retains suitably around 40%.

The low current efficiency of Zn^{2+}+Mn^{2+} coelectrodeposition has always been an important problem that has puzzled researchers[51,54]. Therefore, investigating the cause of low current efficiency and finding ways to improve current efficiency have been the focus items explored by researchers. Fig.7b shows the relationship between the total Zn^{2+}+Mn^{2+} concentration in the electrolyte solution and the current efficiency of theZn^{2+}+Mn^{2+} coelectrodeposition when the molar ratio of Mn^{2+} to Zn^{2+} is constant at 11/9. The total ion concentration increases, but the current efficiency no longer changes enhancedly with the increase of total ion concentration beyond 0.5 M. The current efficiency of Zn^{2+}+Mn^{2+} coelectrodeposition is actually the competition between metal electrodeposition and hydrogen evolution and other side reactions. Increasing the total concentration of Zn^{2+}+Mn^{2+} is conducive to increasing the deposition rate. Properly increasing the total Zn^{2+}+Mn^{2+} concentration can improve the cathode current efficiency, but it is equivalent to increasing the absolute concentration of Mn, so that the H_2 precipitation causes the current efficiency to decrease.

Fig.7c (no adding aloe vera) and Fig.7d (adding aloe vera) shows the effect of the molar ratio of Mn^{2+} to Zn^{2+} on the cathode current efficiency when the total Zn^{2+}+Mn^{2+} concentration in the electrolyte solution is 0.5 M constantly. The total H_2 evolution during the deposition was collected in a burette, and the H_2 gas volume was determined and applied to calculate the current density related to the H_2 evolution reaction using Faraday's law[66-68]. Ultimately, the current efficiency for deposition was calculated by subtracting the current density related to H_2 evolution from the total current density employed. Showed in the Fig.7c and Fig.7d, the low molar ratio provides yet higher current efficiency than that of high molar ratio, and much higher than that of previous research report with another system[40]. Then as the molar ratio increases, the current efficiency declines. When the molar ratio reaches 1/1 to 4/1, the current efficiency drops to a minimum level. Subsequently, as the molar ratio keeps on increasing, the current efficiency increases to some extent. The curve d with adding aloe vera as bio-plasticizer in basic solution is more obvious, which indicates the reason that aloe vera can improve the current efficiency of Zn^{2+}+Mn^{2+} coelectrodeposition may be caused by the increase of Mn^{2+} deposition. Showed in Fig.A, the surface particles of the Zn-Mn alloy electrodeposited without adding aloe vera are coarse, the morphology have clear cauliflower-like clusters of globular crystallites. The massive circular clusters of globules form gas holes during the evolution of H_2 bubbles. However the aloe vera is contained in the electrolyte solution, Showed in Fig.B, the surface condition of the deposits is significantly improved, the alloy structure is uniform and dense, the grains are very fine, the grain boundaries are small, and segregation, crystal defects, such as dislocations, are reduced, which greatly reduces the corrosion of microbatteries. The structure and morphology are rendered by the leveling effect of bio-plasticizer, which may favor the Mn depositing on cathode and inhibiting the H_2 generating, and acccompanied higher current efficiency. When the electrolyte solution is a pure Mn^{2+} solution, the current efficiency can also reach about 70%. The current efficiency of Zn^{2+}+Mn^{2+} coelectrodeposition is much lower than that of pure Zn electrodeposition, and it is not much different from that of pure Mn electrodeposition. Therefore, we can draw the conclusion that the current efficiency of Zn^{2+}+Mn^{2+} coelectrodeposition is limited by the current efficiency of Mn^{2+} electrodeposition. The higher the proportion of Mn^{2+} in the electrolyte solution or the higher the Mn at% in the layer, the lower the current efficiency, which indicates that the Mn^{2+} electrodeposition dominates the current efficiency of Zn^{2+}+Mn^{2+} electrodeposition.

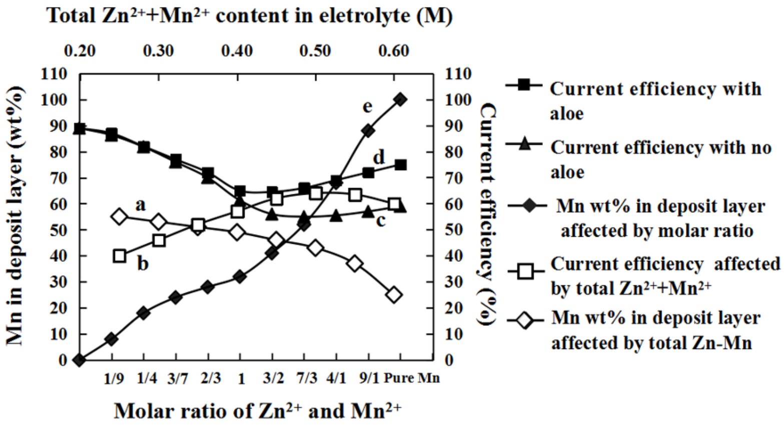

Figure 7. Influence of molar ratio of Zn to Mn and total Zn^{2+}+Mn^{2+} concentration in electrolyte on Mn wt% in deposition layer and cathode current efficiency at 30℃ temperature and pH 6. The basic solution containing: 0.6 M Na_3Ct, 0.4 M H_3BO_3, 0.2 M KCl

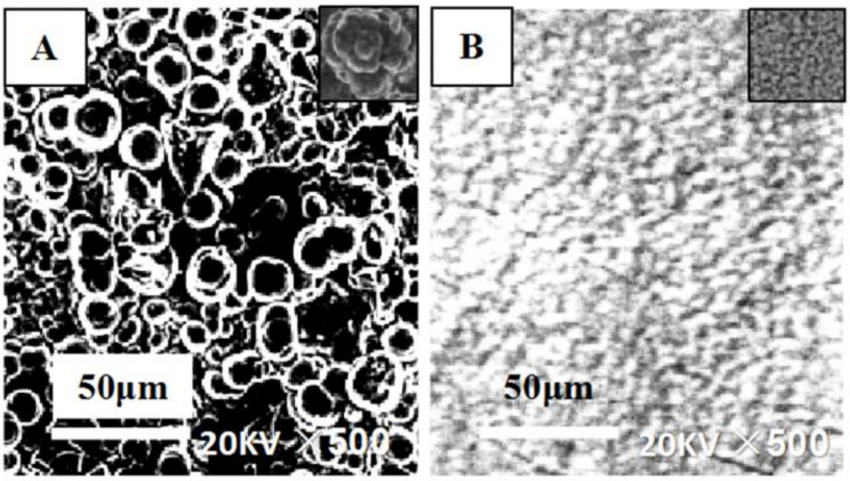

Figure 8. SEM images of Zn-Mn eletrodeposits of D_k 3.5 A.dm^{-2} at 30℃ temperature, pH 6 produced potentiostatically from the solution containing 0.4 M $ZnCl_2$+$MnCl_2$ (the molar ratio 1/1), 0.6 M Na_3Ct, 0.4 M H_3BO_3, 0.2 M KCl, with: A, 3g/L Aloe vera as bio-plasticizer; B, no Aloe vera

Considering the current efficiency, corrosion resistance, hydrogen evolution, and surface morphology, the optimal concentration of $ZnCl_2$+$MnCl_2$ in the electrolyte should be 0.5 M as the molar ratio of Mn^{2+} to Zn^{2+} maintained 11/9, and the aloe vera employed as bio-plasticizer. The porous carbon felt-supported Zn-Mn alloy electrode was fabricated by coelectrodeposition in the confirmed electrosolution. The porous carbon felt matrices provide a high specific area, and the three-dimensional surfaces serve to enlarge the accessible reaction area and enhance the loading capacity of Zn and Mn.

3.5 Charge-discharge performance of a porous carbon-supported Zn-Mn//Mn-doped PANI suspension flow battery

The 3D Zn-Mn alloy //Mn-doped PANI suspension flow battery was designed as follows. The Mn-doped PANI suspension was used as the cathode active material, and the prepared 3D Zn-Mn alloy was used as the anode. The mixed solution contained 0.3 M $MnCl_2$, 0.5 M $ZnCl_2$, 0.3 M NH_4Cl and 0.1 M LiCl as the electrolyte. The charge/discharge performance for the present battery was investigated. During the charging process, Mn^{2+} and Zn^{2+} cations in the electrolyte solution were deposited on the 3D porous carbon felt, and the PANI cathode was oxidized with Cl^- doping. During discharge, the Mn and Zn dissolved in the electrolyte, and the PANI particles were reduced with the release of Cl^-.

To investigate the present battery performance, a constant current charge-discharge experiment was carried out at current densities of 15 mA cm^{-2}, 20 mA cm^{-2}, and 30 mA cm^{-2} for cell voltages ranging from 0.7 V to 1.9 V, as shown in Fig. 7. As shown in Fig. 9, there were well-defined charge/discharge curves, and the battery presented a smooth discharge platform for the cell voltage ranging from 1.4 V to 1.0 V regardless of the current strength. At a current density of 15 mA cm^{-2}, the maximal cell capacity density reached 153 mAh·g^{-1}, higher than the theoretical value of PANI, which was mentioned in another paper[69]. This difference may be due to the easy oxidation of the lecouemeraldine base form of PANI into the emeraldine base form, which resulted from reoxidation by oxygen in the environment of reduced

PANI microparticles after the discharge process[70-71]. Compared to the transition PANI composite film battery, the present battery design is expected to operate at a high discharge current for high output power. The Zn//PANI suspension flow battery with a Zn plate as the anode suffered from a low average operating voltage of 0.8 V. In contrast, the present battery that uses Zn-Mn alloy as the anode provides an average discharge voltage of approximately 1.2 V, and the maximal operating voltage reached 1.7 V. The discharge capacity after increasing the current density decreased from 153 mAh·g^{-1} to 95 mAh·g^{-1}, which may reflect the loss of doped Mn or electrochemical degradation of the cathode material owing to overoxidation of PANI. In addition, the coulombic efficiency of the charge/discharge cycle was far greater than 100%, i.e., 122.4% at 15 mA cm^{-2}, which was due to the oxidation of reduced PANI by oxygen in the air before charging.

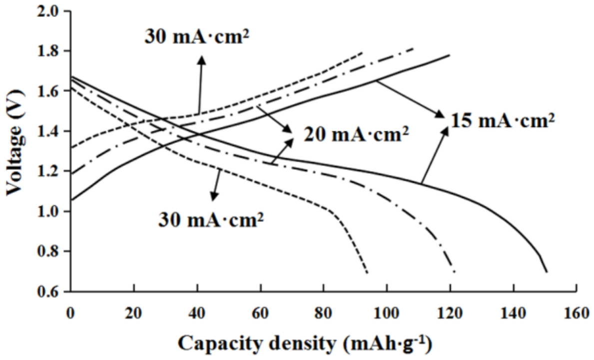

Figure 9. Charge-discharge capacity density of the present battery at various current densities.

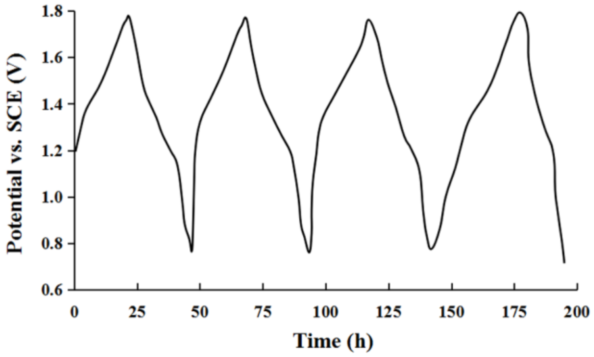

Figure 10. Charge-discharge time-potential for the present battery at a constant current density of 15 mA·cm^{-2}.

Fig. 10 shows the charge-discharge response during repeated cycles at 15 mA cm^{-2}. The cell potential-time curves exhibited similar defined shapes during four repeated cycles of charge/discharge. The battery charging started at approximately 1.2 V, and the time potential rapidly increased at the initial stage. This increase was followed by a slow increase in the potential until a peak at 1.8 V. The discharge process began at 1.6 V and presented a smooth decrease from 1.4 V to 1.0 V. The cell discharge capacity density was 117.3 mAh·g^{-1} in the first charge/discharge process and gradually decreased to 114.5 mAh·g^{-}

^{1} after four cycles. Since the cell operates in an open system, the discharge capacity density is negligibly attenuated due to environmental factors such as changes to the solution due to water evaporation[50]. Therefore, the designed battery offers fine cycle performance, demonstrating excellent potential for application.

4. CONCLUSION

We have demonstrated improved electroactivity of PANI by utilizing a $MnCl_2$ aqueous solution as the electrolyte. A LiCl additive promoted low solution acidity and indirectly limited corrosion of the anode. The addition of $MnCl_2$ during the PANI electropolymerization process improved the PANI activity. Coelectrodeposition was successfully applied to the fabrication of a 3D Zn-Mn alloy anode, and an appropriate total $ZnCl_2$+$MnCl_2$ concentration and a suitable molar ratio of Mn to Zn in solution improved the codeposition efficiency. The battery tests showed that the 3D Zn-Mn//Mn-doped PANI suspension flow battery possessed good electrochemical properties and stable cycling performance. The average discharge voltage of the present battery was 0.4 V higher than that of a transitional Zn//PANI suspension flow battery. The specific capacity of the cell reached 153 $mAh\cdot g^{-1}$ at a current density of 15 mA cm^{-2}. This value is more than the theoretical value of PANI, indicating that the present battery is expected to operate at a high discharge current for high output power. If the working environment for the battery is optimized, the attenuation of the battery discharge capacity density is expected to be very low.

ACKNOWLEDGEMENT
The authors are grateful to the Nature Science Foundation of China (No.21727810), the Nature Science Foundation of Hunan Science and Technology Department (No.2018JJ5024) for financial support.

CONFLICTS OF INTEREST
There are no conflicts to declare.

References

1. K.Wang. J.Y. Huang, Z.X. Wei, *J. Phys. Chem. C.*, 114 (2010) 8062.
2. M.A.I. Shuvo, M.A.R. Khan, H. Karim, P. Morton, T. Wilson, Y.R. Lin, *ACS Appl. Mater. Interface*, 16 (2013) 7881.
3. H.L. Liu, Y. Wang, X.L. Gou, T. Qi, J. Yang, Y.L. Ding, *Mater. Sci. Eng. B*, 178 (2013) 293.
4. V. Presser, C.R. Dennison, J. Campos, K.W. Knehr, E.C. Kumbur, Y. Gogotsi, *Adv. Energy Mater.*, 7 (2012) 895.
5. Q. Lu, Q. Zhao, H.M. Zhang, J. Li, X.H. Wang, F.S. Wang, *ACS Macro. Lett.*, 2 (2013) 92.
6. G.H. El-Nowihy, A.M. Mohammad, M.M.H. Khalil, M.A. Sadek, M.S. El-Dead, *Int. J. Electrochem. Sci.*, 12 (2017) 40.
7. M.S. Rahmanifar, M.F. Mousavi, M. Shamsipur *J. Power Sources*, 110 (2002) 229.
8. A. Mirmohseni, R. Solhjo, *Eur. Polym. J.* 39 (2003) 219.
9. M.S. Rahmanifar, M.F. Mousavi, M, Shamsipur, H. Heli, *Synth. Met.*, 155 (2005) 480.
10. J.F. Mike, J.L. Lutkenhaus, *J. Polym. Sci. Part B: Polym. Phys.*, 51 (2013) 468.
11. Y.F. Zhao, S.S.Si, C. Liao, *J. Power Sources*, 241 (2013) 449.

12. S. Wu, Y.F. Zhao, D.G. Li, *J. Power Sources*, 275 (2015) 305.
13. D.G. Li. S. Wu, Y. Xia, S. S. Si, *J. Xuzhou Inst. Tech.*, 30 (2015) 35.
14. Y. Xia, D.G. Li, S. S. Si, *J. Power Sources*, 283 (2015) 125.
15. D.C. Trivedi, *J. Solid State Electrochem.*, 2 (1998) 85.
16. J.Z. Jiang, F.G. Meng, Y.G. Tang, *Nonfer. Met.*, 55 (2003) 21.
17. X.Y. Sun, D.B. Zhou, L.H. Tan, *Appl. Chem. Ind.*, 39 (2010) 37.
18. L.C. Zhou. *Manga. Ind. China.* 10 (1992) 42.
19. P. Ilea, I.C. Popescu, *Hydrometallurgy*, 46 (1997) 149.
20. W.P. Li, S.T. Zhang, L.T. Yang, Z.D. Wei, *Acta Chim. Sinica*, 67 (2009) 529.
21. W. P. Li, S.T. Zhang, Appl. Surf. Sci., 257 (2011) 3275.
22. W. P. Li, *Chongqing U. J.*, 4 (2011) 1
23. P. Yang, R.L. Man, P.F. Zhao, *J. Chem. Ind & Eng.*, 33 (2012) 45.
24. N. Galvanauskaite, A. Sulcius, E. Griskonis, P. Diaz-Arista, *Trans. Inst, Met. Finish.*, 89 (2011) 325.
25. M. Osial, J. Widera, K. Jackowska, *J. Solid State Electrochem.*, 17 (2013) 2477.
26. J.M. Lu, D. Dreidinger, T. Glück, *Hydrometallurgy*, 141 (2014) 105.
27. T. Pandiyarajan, R.V. Mangalaraja, B. Karthikeyan, *Spectrochimica Acta A,* 147 (2015) 280.
28. M.N. Anjum, L.H. Zhu, Z.H. Luo, J.C. Yan, H.Q. Tang, *Polymer*, 52 (2011) 5795.
29. L.C.Fonseca, R. Faez, F.F.Camilo, M.A. Bizeto, *Micropor. Mesopor. Mater.*, 159(2012) 24.
30. Z.Q. Huang, L. Li, Y.F. Wang, C. Zhang, T.X. Liu, *Compos. Commun.*, 8 (2018) 83.
31. X.X. Gong, G.T. Fei, W.B. Fu, M. Fang, X.D. Gao, B.N. Zhong, L.D. Zhang, *Org. Electron.*, 47 (2017) 51.
32. Z. Huang, C.L. Huang, X. Luo, *Solid State Commun.*, 276 (2018) 37.
33. S.Y. Wang, Y.N. Li, J. Wang, S.X. Wang, Q.Shi, Z.C. Tan, *Thermochim Acta*, 658 (2017) 7.
34. R.B. Patil, A.A. Jatratkar, R.S. Deven, Y.R. Ma, R.K. Puri, V. Puri, J.B. Yadav, *Appl Surf Sci.*, 327 (2015) 201.
35. R. Yuksel, C. Durucan, H.E. Unalan, *J. Alloy Compd.*, 658 (2016) 183.
36. H.L. Cheng, C.B. Hu, X.G. Wang, Z.Q. He, Int. *J. Electrochem. Sci*, 13 (2018) 196.
37. R.F. Hu, J. Zhao, G.D. Zhu, J.P. Zheng, *Electrochim Acta.*, 261 (2018) 151.
38. Y.L. Tian, S.L. Dou, X. Zhang, L.P. Zhang, L.L. Wang, J.P. Zhao, X. Zhao, Y. Li, *Synthetic Met.*, 232 (2017) 111.
39. H. Xu, J.L. Zhang, Y. Chen, H.L. Lu, *J. Solid State Electrochem*, 18 (2014) 813.
40. H.J. Cao, S.H. Si, X.B. Xu, J.R. Li, Y. X, J. Electrochem. Soc., 166 (2019) A1266-A1274.
41. Y.T. Shieh, J.J. Jung, R.H. Lin, C.H. Yang, T.L. Wang, *Electrochim. Acta*, 70 (2012) 331.
42. Q.M. Jia, L.H. Jiang, Y.M. Wang, *Rare Met. Mater. Eng.*, 39 (2010) 538.
43. K.B. Hatzell, L.Fan, B. Majid, *ACS Appl. Mater. Interfaces*, 6 (2014) 8886.
44. H. Wang, Z. Liu, H.Y. Li, J. Electrochem. Sci., 13 (2018) 136.
45. D.S. Patil, J. Shaikh, D. Dalavi, M.M. Karanjkar, J. Electrochem. Soc., 158 (2011) A653.
46. D.S. Patil, S.A. Pawar, V.B. Mamlayya, R.S. Devan, Y.R. Ma, P.S. Patil, Journal of Shivaji University (Science & Technology), 41(2014-2015)14.
47. J.B.M Krishna, A. Saha, G.S. Okram, A. Soni, S. Purakayastha, B. Ghosh, J. Phys. D: Appl. Phys. 42 (2009) 9.
48. A. Gupta, M. Kumar, J. Mater. Sci. Eng., 6 (2017) 2.
49. A. Gupta, M. Kumar, J. Mater. Sci. Surf. Eng., 6 (2018) 802.
50. Y. Xia, D.R. Zhu, S.H. Si. *J. Power sources*, 283 (2015) 125.
51. N. Loukil, M. Feki, *Appl, Surf. Sci.*, 410 (2017) 574.
52. N. Loukil, M. Feki, *J. Alloy. Compd.*, 719 (2017) 420.
53. K. Tominaga, W.Takashima, K. Kaneto, *Thin Solid Films*, 519 (2010) 978.
54. S. Ganesan, G. Prabhu, B.N. Popov, *Surf. Coat. Technol.*, 238 (2014) 143.
55. M. Bučko, J. Rogan, S.I. Stevanović, S. Stanković, J.B. Bajat, *Surf. Coat. Technol.*, 228 (2013)

221.
56. M. Ramasubramanian, B.N. Popov, R.E. White, *J. Electrochem. Soc.*, 145 (1998) 1907.
57. P. Ganesan, S.P. Kumaraguru, B.N. Popov, *Surf. Coat. Technol.*, 201 (2007) 7896.
58. H. Kim, B.N. Popov, K.S. Chen, *J. Electrochem. Soc.*, 150 (2003) C81.
59. H. Kim, B. Popov, K.S. Chen, *Corros. Sci.,* 45 (2003) 1505.
60. P. Ganesan, S.P. Kumaraguru, B.N. Popov, *Surf. Coat. Technol.,* 201 (2006) 3658.
61. C.J. Lan, W.Y. Liu, S.T. Ke, T.S. Chin, *Surf. Coat. Technol*., 201 (2006) 3103.
62. A.P. Yadav, H. Katayama, K. Noda, H. Masuda, A. Nishikata, T. Tsuru, *Corros. Sci.*, 49 (2007) 3716.
63. J.B. Bajat, S. Stanković, B.M. Jokić, S.I. Stevanović, S*urf. Coat. Technol.,* 204 (2010) 2745.
64. S. Dubent, M.L.A.D. Mertens, M. Saurat, *Mater. Chem. Phys.*, 120 (2010) 371.
65. P.S.D. Silva, E.P.S. Schmitza, A. Spinelli, J.R. Garcia, *J. Power Sources*, 210 (2012) 116.
66. M. Bučko, J. Rogan, B. Jokić, M. Mitrić, U. Lačnjevac, J.B. Bajat, *J. Solid State Electrochem.*, 17 (2013) 1409.
67. S. Fashu, C.D. Gu, J.L. Zhang, H. Zheng, X.L. Wang, J.P. Tu, *J. Mater. Eng. Perform.*, 24 (2015) 434.
68. D. Sylla, J. Creus, C. Savall, O. Roggy, M. Gadouleau, P. Refait, *Thin Solid Films*, 424 (2003) 171.
69. A. Janošević, L. Pašti, N. Gavrilov, S. Mentus, J. Krstić, M. Mitrić, J. Travas-Sejdic, G. Ćirić-Marjanović, Micr*opo. Mesopo. Mater.*, 152 (2012) 50.
70. G. Ćirić-Marjanović, *Synthetic Met.*,177 (2013) 1.
71. A. Gabe, M.J. Mostazo-López, D. Salinas-Torres, E. Morallón, D. Cazorla-Amorós, *Hybrid Polymer composite Material*, (2017) 173.